# RESEARCH ARTICLE

**Key Points:**
- Breach openings and widening caused by large pressure gradient driven flows during three hurricanes
- Breach closure after a period of large alongshore sediment flux and small ocean-bay pressure gradients
- Winds are a major control on ocean-bay pressure gradients

**Correspondence to:**
I. Safak,
isafak@usgs.gov

# Barrier island breach evolution: Alongshore transport and bay-ocean pressure gradient interactions

**Ilgar Safak[1], John C. Warner[1], and Jeffrey H. List[1]**

[1]U.S. Geological Survey, Woods Hole Coastal and Marine Science Center, Woods Hole, Massachusetts, USA

**Abstract** Physical processes controlling repeated openings and closures of a barrier island breach between a bay and the open ocean are studied using aerial photographs and atmospheric and hydrodynamic observations. The breach site is located on Pea Island along the Outer Banks, separating Pamlico Sound from the Atlantic Ocean. Wind direction was a major control on the pressure gradients between the bay and the ocean to drive flows that initiate or maintain the breach opening. Alongshore sediment flux was found to be a major contributor to breach closure. During the analysis period from 2011 to 2016, three hurricanes had major impacts on the breach. First, Hurricane Irene opened the breach with wind-driven flow from bay to ocean in August 2011. Hurricane Sandy in October 2012 quadrupled the channel width from pressure gradient flows due to water levels that were first higher on the ocean side and then higher on the bay side. The breach closed sometime in Spring 2013, most likely due to an event associated with strong alongshore sediment flux but minimal ocean-bay pressure gradients. Then, in July 2014, Hurricane Arthur briefly opened the breach again from the bay side, in a similar fashion to Irene. In summary, opening and closure of breaches are shown to follow a dynamic and episodic balance between along-channel pressure gradient driven flows and alongshore sediment fluxes.

## 1. Introduction

Breaches through barrier islands can be formed by several processes including dune face erosion or by dune overtopping that allows flow across the island. Breaches can have positive ecological and economical effects by increasing water exchange between the ocean and the bay that will alter water quality and potentially provide navigational routes and reduce flooding hazards, and by providing sediment to adjacent shorelines and transitional routes to species [e.g., *Castelle et al.*, 2007]. However, their formation may also cause damage to coastal infrastructure. Two competing hydrodynamic processes controlling inlet evolution are thought to be tides, and alongshore sediment flux due to waves that break with an oblique angle with respect to shore normal, i.e., littoral drift [e.g., *De Swart and Zimmerman*, 2009]. Littoral drift, part of which is interrupted by the tidal inlet flows and transported into the inlet, tends to close an inlet [*Smith and Zarillo*, 1988]. Tidal currents, on the other hand, tend to scour the inlet and keep it open [*De Swart and Zimmerman*, 2009]. In a bay system with a geomorphically stable well-defined inlet to the ocean, stability of the inlet can be approximated using simple relations between the tidal prism of the bay, the inlet cross section, and the annual total littoral drift arriving at the inlet [e.g., *Bruun and Gerritsen*, 1960; *Walton and Adams*, 1976; *Tung et al.*, 2009]. Recent investigations also highlight possible contribution of wave-induced onshore sediment transport to inlet closure, in environments with relatively weak littoral drift [*Ranasinghe et al.*, 1999]. In addition, simple approximations do not account for extreme events (hurricanes, energetic storms with high surge) which may also open a breach due to water elevation differences between the lagoon and the ocean sides where the water level reaches the top of the barrier beach [*Kraus et al.*, 2008]. Therefore, the processes leading to initial opening, as well as closure, of barrier island breaches are not well understood.

The Outer Banks of North Carolina are a chain of barrier islands which separate Pamlico and Albemarle Sounds from the Atlantic Ocean (Figure 1) and have been impacted by storms and hurricanes. These islands have experienced breaches numerous times. One location that has recently had successive breaches and closures is near the Pea Island National Wildlife Refuge (referred as Pea Island breach, hereafter) located approximately 10 km South of the Oregon Inlet in North Carolina (Figure 1).
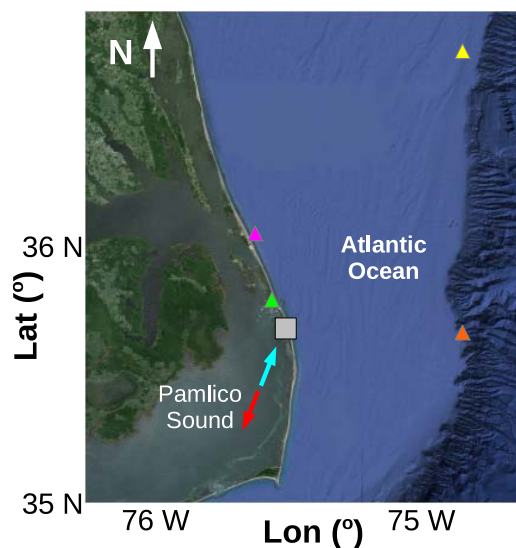
**Figure 1.** Atlantic Ocean, Outer Banks along the North Carolina coast of USA, and Pamlico Sound (Image courtesy: Landsat, Google Earth, 2016). Grey rectangle highlights the Pea Island breach location shown in detail in Figures 2 and 3. Green, magenta, orange and yellow triangles correspond to the locations of wind and water level measurements at the bay side (NOAA gauge 8652587), water level measurements at the ocean side (NOAA gauge 8651370), WaveWatch III deep-water wave estimates, and wave measurements (NDBC buoy 44014), respectively; red and cyan arrows show the orientations of winds blowing from the dominant wind directions NNE and SSW, respectively.

Opening and evolution of the Pea Island breach were interpreted using photographs in previous studies [*Clinch et al.*, 2012; *Overton and Smyre*, 2013; *Velasquez et al.*, 2015] but these studies did not include an in-depth analysis of the driving physical processes. Based on communications with both North Carolina Department of Transportation (NCDOT) and U.S. Fish and Wildlife Service, it is assured that the system evolves due to natural processes with no human intervention (no beach nourishment or sand pumping, etc.). This study examines the physical processes that have opened and closed the Pea Island breach since 2011, during which three hurricanes impacted the area. Hurricane Irene made landfall near Cape Lookout, NC (about 160 km Southwest of Pea Island) with a low-pressure of about 950 mbar on 27 August 2011, and traveled across the Pamlico Sound and opened the Pea Island breach. Hurricane Sandy became Category 2 offshore of Cape Hatteras, NC (about 55 km South of Pea Island) with winds exceeding 42 ms$^{-1}$ on 29 October 2012 while it was traveling along the US East Coast. Hurricane Arthur, which had a much shorter duration compared to these two hurricanes, made landfall between Cape Lookout and Beaufort on 3 July 2014.

Our hypothesis is that the timing and relative importance of breach-opening energetic events (such as hurricanes triggering pressure gradient-driven flows due to water level gradients between the bay and the ocean) and alongshore transport events are critical to controlling the evolution and eventual closure of a breach. To test this hypothesis, atmospheric and oceanographic data near the Pea Island breach location and aerial photographs of the area taken between 2011 and 2015 are analyzed. Using the wind and water level data sets at the Pamlico Sound and Atlantic Ocean sides of the breach, pressure gradients between the ocean and the bay and the resulting along-channel sediment transport are estimated. Wave parameters from offshore buoys and model hindcasts are used for modeling alongshore sediment transport rates along the ocean side of the Pea Island. The results are analyzed to investigate the evolution of the breach due to these two processes; i.e., along-channel (cross-island) pressure gradient and alongshore sediment transport at the breach location.

## 2. Data

Data were acquired for both conceptual and deterministic evaluations. Aerial photographs of the breach location (Figure 2), provided by the NCDOT Photogrammetry Unit, were used to evaluate timing of breach openings and closures, and assess inlet stability. Topography near the Pea Island breach before and after Hurricane Irene (Figure 3) was analyzed using the LIDAR data obtained from National Oceanic and Atmospheric Administration (NOAA) Coastal Services Center [*Hardin et al.*, 2012]. Water levels (Figure 4) were obtained from the NOAA gage at the Oregon Inlet Marina Station (ID:8652587) for the bay side (green triangle in Figure 1) and the Duck Pier Station, located at about 300 m offshore (ID:8651370), for the ocean side (magenta triangle in Figure 1). Water levels were converted to the North American Vertical Datum 1988 (NAVD 88) for comparison between sites. Wind data (Figure 4) were also obtained from the Oregon Inlet Marina Station (green triangle in Figure 1). Wave parameters for 2011–2015 (Figure 5) were extracted from the hindcasts of the third-generation WaveWatch III model [*Tolman*, 2009] on its 4 min-resolution Atlantic Ocean grid, at about 300 m depth at 60 km East of Pea Island (orange triangle in Figure 1) and at the location of a nearby wave buoy. The performance of WaveWatch III near the study site was evaluated based on the wave observations at the closest NOAA National Data Buoy Center (NDBC) Station that provided data

**Figure 2.** (a–i) Aerial photographs of the Pea Island breach location with dates indicated (also highlighted in Figures 4 and 10). Photographs cover the same area that is about 800 m wide and 1000 m long. Red lines are given as reference to the initial extent of the breach after Hurricane Irene (a). Magenta arrows in Figure 2a show the alongshore and along-channel directions. The aerial photographs are courtesy of the NCDOT Photogrammetry Unit.

for the study period. NDBC Buoy ID:44014 is located at 48 m water depth, approximately 110 km Northeast of Pea Island (yellow triangle in Figure 1). The model-data comparison shows that the WaveWatch III model results at that location, for wave height (Figure 5a), period (Figure 5b) and direction (Figure 5c), agree well with the observations there. $r^2=0.86$ (Figure 6) with an Index of Agreement [*Willmott et al.*, 1985] of 0.96
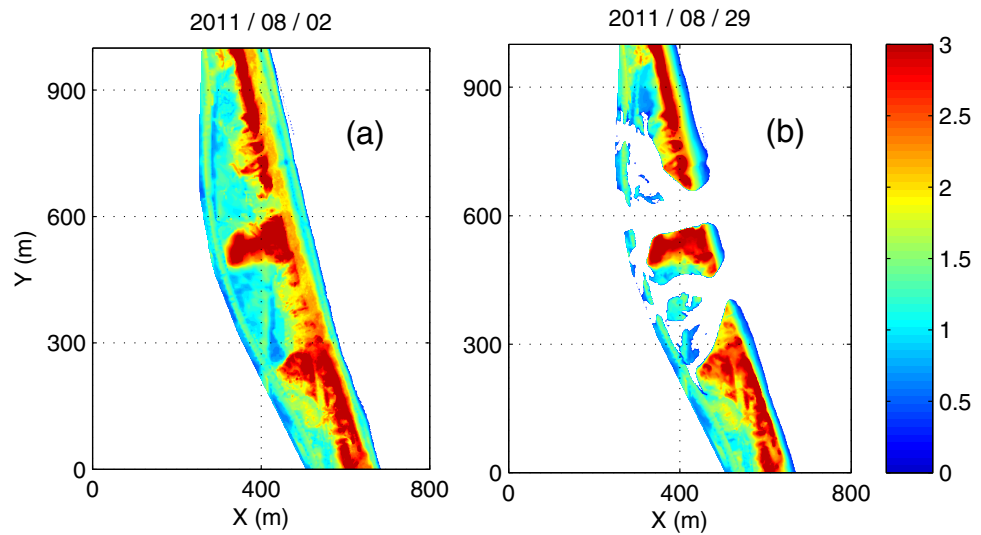
**Figure 3.** Topography (with respect to NAVD 88) near Pea Island (a) before and (b) after Hurricane Irene.

(value of 1 indicates perfect agreement). Therefore, WaveWatch III is expected to have a good performance offshore of Pea Island. All these observations of winds, water levels and waves, and model hindcasts of waves are open source and available online (detailed in Acknowledgments).
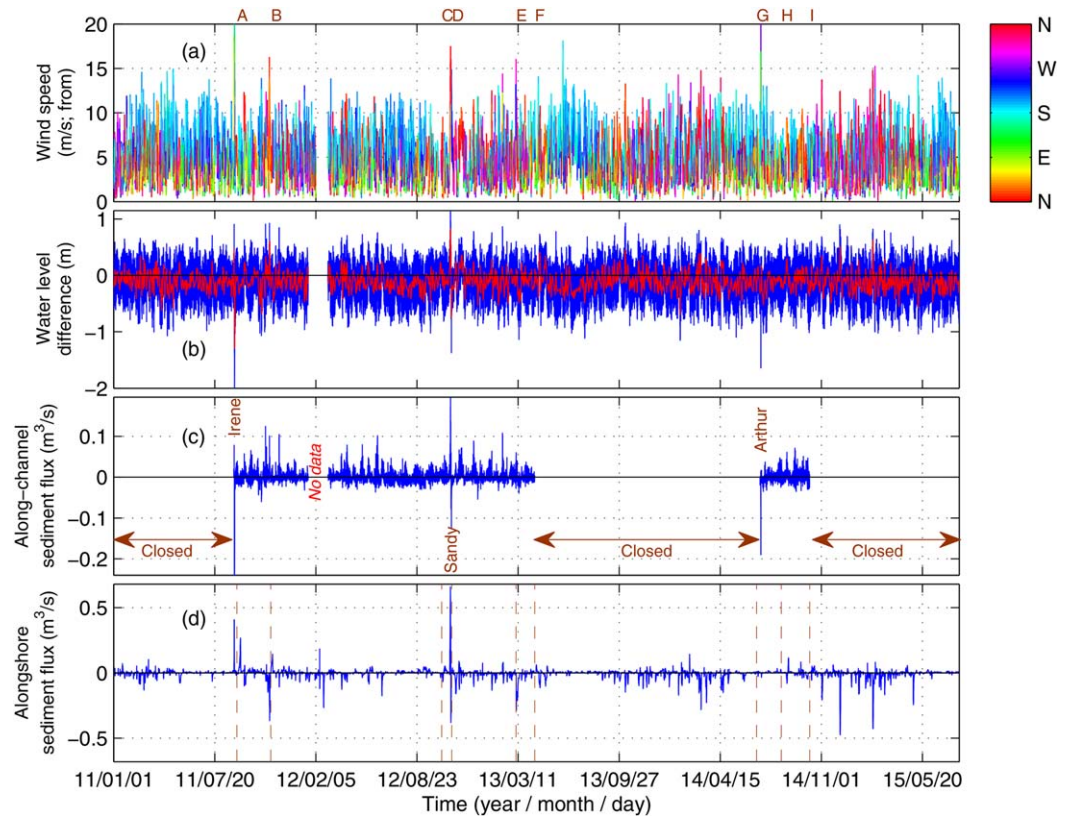


**Figure 4.** General conditions near Pea Island between 2011 and 2015: (a) Wind speed and direction (colors indicate the direction winds are from; e.g., red means Northerly winds); (b) water level differences between the ocean and the bay sides (positive means the ocean water level is higher than the bay; blue and red curves show the raw data and the 30 h low-pass-filtered data, respectively); (c) sediment transport rate along the channel (across the island; positive and negative indicate flux toward the bay and toward the ocean, respectively); (d) sediment transport rate along the Pea Island, across the Pea Island breach (positive and negative indicate Northward transport and Southward transport, respectively). Capital letters at the top of the figure and the brown dashed lines in Figure 4d indicate the dates of the photographs shown in Figure 2. The gap near February 2012 in the curves on Figures 4b and 4c is due to absence of water level observations.
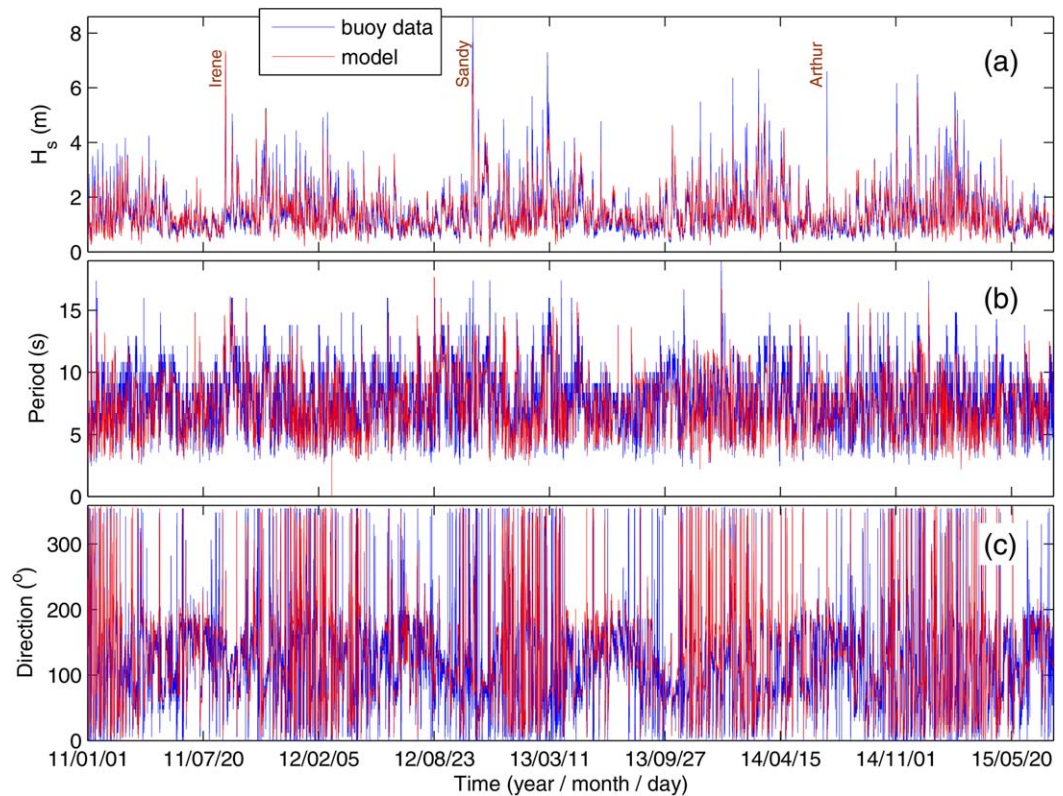
**Figure 5.** Wave conditions offshore of Pea Island between 2011 and 2015: (a) Significant wave height; (b) wave period; and (c) wave direction (indicating the direction waves are from, clockwise from North which is zero; e.g., 90° means waves from the East). Blue and red curves show the observations at the NDBC 44014 buoy at 48 m depth (yellow triangle in Figure 1) and the wave model results at that location, respectively. The times of the three hurricanes are indicated with their names in Figure 5a.
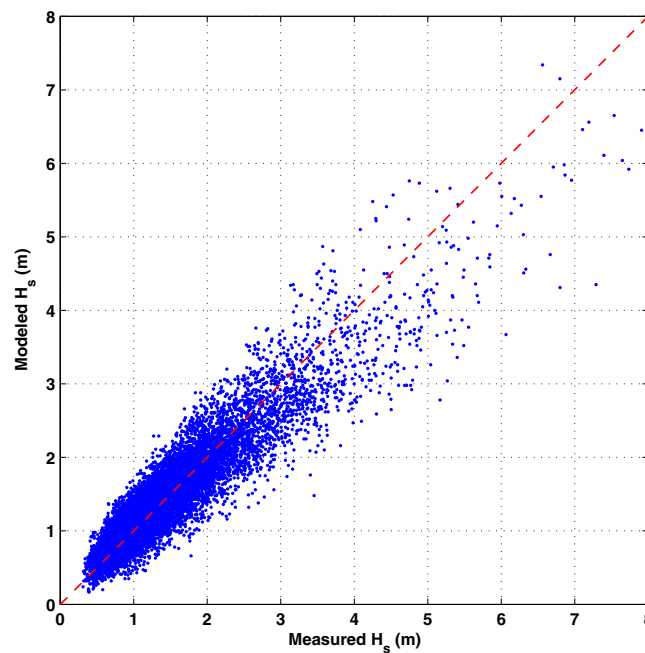


**Figure 6.** Comparison of the modeled significant wave heights with the observations at the NDBC 44014 buoy. Red dashed line shows the one-to-one relationship.

## 3. Methods

Wave-induced alongshore (orientation indicated with magenta arrow in Figure 2a) sediment transport rates along the location of the Pea Island breach ($Q$ in $m^3 s^{-1}$) are estimated as [*Ashton and Murray*, 2006]:

$$Q = K H_o^{2.4} T^{0.2} \cos^{1.2}(\phi_o - \theta) \sin(\phi_o - \theta), \quad (1)$$

where $K$ is an empirical constant, $H_o$, $T$, and $\phi_o$ are deep water wave height, period and wave angle relative to shoreline, and $\theta$ is the shoreline orientation. $K$ is taken as 0.34 from the literature and its magnitude does not affect the conclusions here. For Pea Island, $\theta$ is about 13 degrees counter-clockwise from North (Figures 1–3).

The pressure gradients between the ocean and the bay are estimated based on the water level observations. These pressure gradients are then used for

estimating along-channel (orientation indicated with magenta arrow in Figure 2a) flow. The depth-averaged along-channel momentum balance is given as:

$$\frac{\partial u}{\partial t} + u\frac{\partial u}{\partial x} + v\frac{\partial u}{\partial y} = -g\frac{\partial \eta}{\partial x} - C_d\frac{u|u|}{h+\eta} ,$$ (2)

where $u$ is the along-channel velocity, $t$ is time, $x$ is the along-channel distance, $v$ is the cross-channel velocity, $y$ is the cross-channel distance, $g$ is the gravitational acceleration, $\eta$ is the instantaneous water level relative to mean sea level, $C_d$ is the bottom drag coefficient, and $h$ is the mean water depth. Convective and advective accelerations on the left-hand side of equation (2) are balanced by the along-channel pressure gradient and bottom friction on the right-hand side. Assuming steady state and neglecting advection in a narrow and shallow channel give a widely used along-channel momentum balance between the along-channel pressure gradient and bottom friction:

$$g\frac{\partial \eta}{\partial x} = -C_d\frac{u|u|}{h+\eta} .$$ (3)

Scaling of terms in the full momentum balance and derivation of this simplified balance, used in this study also due to the absence of direct measurements of velocity at multiple locations, are discussed in details by *Stigebrandt* [1980] and *Hill* [1994]. Relating the bottom friction term to bottom stress ($\tau$):

$$g\frac{\partial \eta}{\partial x} = -C_d\frac{u|u|}{h+\eta} = \frac{\tau}{\rho(h+\eta)} ,$$ (4)

where $\rho$ is the water density (1025 kg m$^{-3}$) gives for bottom stress:

$$\tau = \rho(h+\eta)g\frac{\partial \eta}{\partial x} .$$ (5)

Then, an estimate of along-channel sediment flux per unit channel width is obtained as [*Meyer-Peter and Mueller*, 1948]:

$$q = 8\left(\frac{\tau}{\rho(s-1)gd} - \theta_c\right)^{3/2}\left(d\sqrt{(s-1)gd}\right) ,$$ (6)

where $s$ is the specific density of the sediment particle (2.65), $d$ is the diameter of the sediment particle (250 $\mu$m) [*Poppe et al.*, 2014], and $\theta_c$ is the critical Shields parameter that is commonly taken as 0.05 [*Madsen and Grant*, 1976]. In the absence of direct observations of sediment concentration and flow velocity, equation (6) is used for estimation of bedload fluxes which are expected to dominate sediment transport in the shallow channel depths herein. Breach bathymetry data collected by NCDOT right after Hurricane Irene show the main channel had a triangular cross section with an average width of 75 m, depth of 1.5 m at the channel center, and side slopes of 0.04 [*Kurum et al.*, 2012]. Because the images for later periods show that the channel rapidly became wider and the goal of this study is to investigate the processes controlling breach evolution in long-term, side slopes of 0.02 are used based on the elevations estimated from the later images. Temporal variation of channel width and depth are then calculated using this slope, a mean water depth in the channel center of $h = 1.5$ m, and changing water levels, $\eta$, using the average of bay- and ocean-side water levels.

## 4. Results

The study site is dominated by winds from SSW and NNE (Figures 4a and 7). Wind speeds reach approximately 10–15 ms$^{-1}$, with occasional peaks up to 20 ms$^{-1}$ during major events (Figure 4a). Waves offshore of Pea Island reach 8 m height and 14 s period at the offshore buoy (48 m depth) during these major events (Figures 5a and 5b). Water level differences (ocean-bay) vary mostly between −1 to 1 m, with larger differences correlating with major wind events (Figure 4b; 28 August 2011; 29 October 2012; 4 July 2014; as labeled in Figure 4c). The other prominent feature in water level differences is the vast majority of negative values of 30 h low-pass-filtered (to remove tide effects) water level differences between the ocean and bay (red curve in Figure 4b). This indicates a net mean flow directed from the bay toward the ocean which is consistent with previous observations done in one channel of Oregon Inlet located 10 km North of the
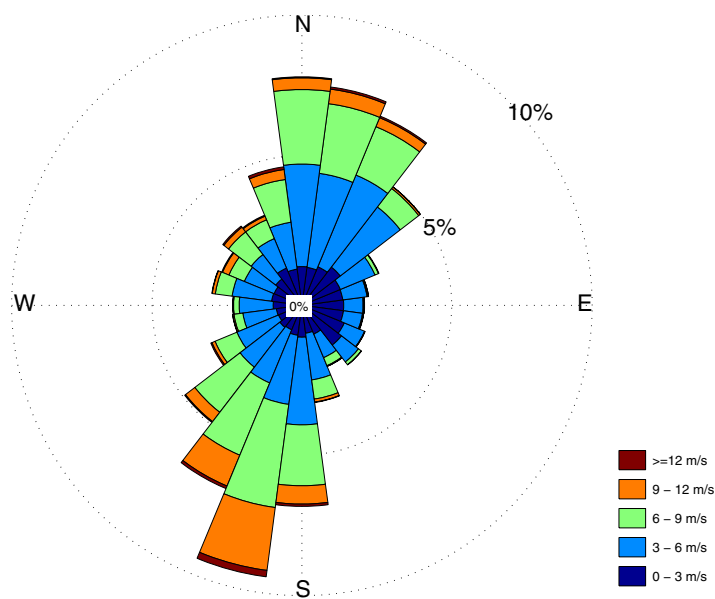
**Figure 7.** Windrose based on the winds measured near Pea Island (green triangle in Figure 1) between 2011 and 2015 (time series shown in Figure 4a).

breach [*Nichols and Pietrafesa*, 1997]. The variation of the water level difference between the ocean and bay as a function of winds becomes more evident using the low-pass-filtered water levels. Figure 8 compares this water level difference to wind direction and shows that the greatest water level differences occur for winds from SSW and NNE. Winds from SSW push bay side water toward Pea Island and increase these water levels to be greater than the ocean side. Winds from NNE, on the other hand, push bay water away from Pea Island and make the bay side water levels be lower than the ocean side. These wind directions are the dominant wind directions in the area

(Figure 7), indicated with the cyan and red arrows on the map in Figure 1. This demonstrates that the bay side water levels and, therefore, ocean-bay pressure gradients are largely controlled by wind direction. This could be expected to be especially true during energetic events considering the major spikes in water level differences during the three hurricanes that significantly impacted the breach (Figure 4b).

The processes that tend to open and maintain the breach can be analyzed by taking a closer look into the three major events of Hurricanes Irene, Sandy and Arthur (Figure 9). Winds during Hurricane Irene exceeded
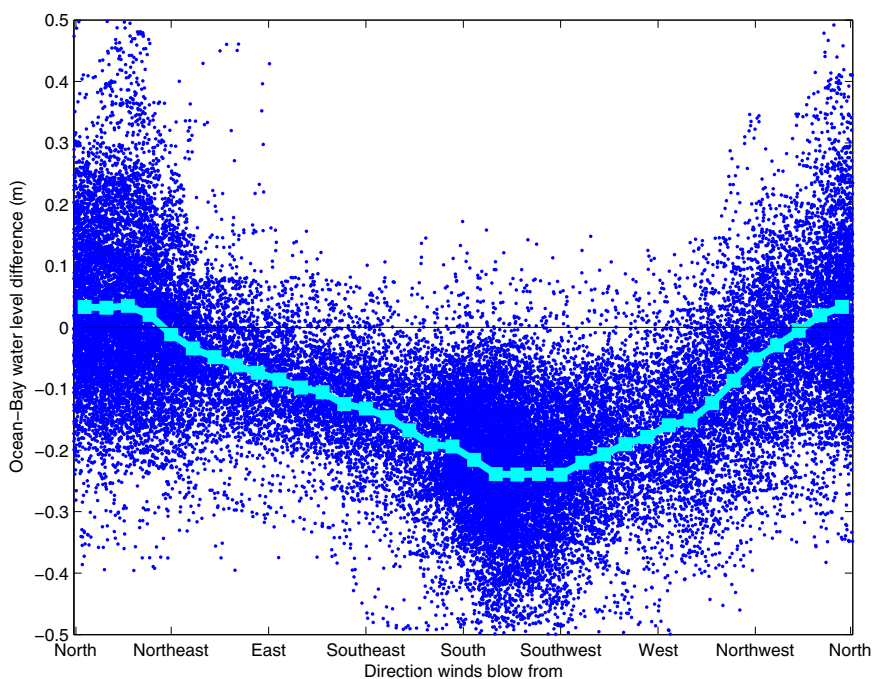


**Figure 8.** Variation of 30 h low-pass-filtered water level differences between the ocean and the bay (red curve in Figure 4b; negative difference means the bay water level is higher than the ocean) as a function of wind direction (color-coded in Figure 4a). Cyan squares indicate the averages over 10°-wide directional bins.
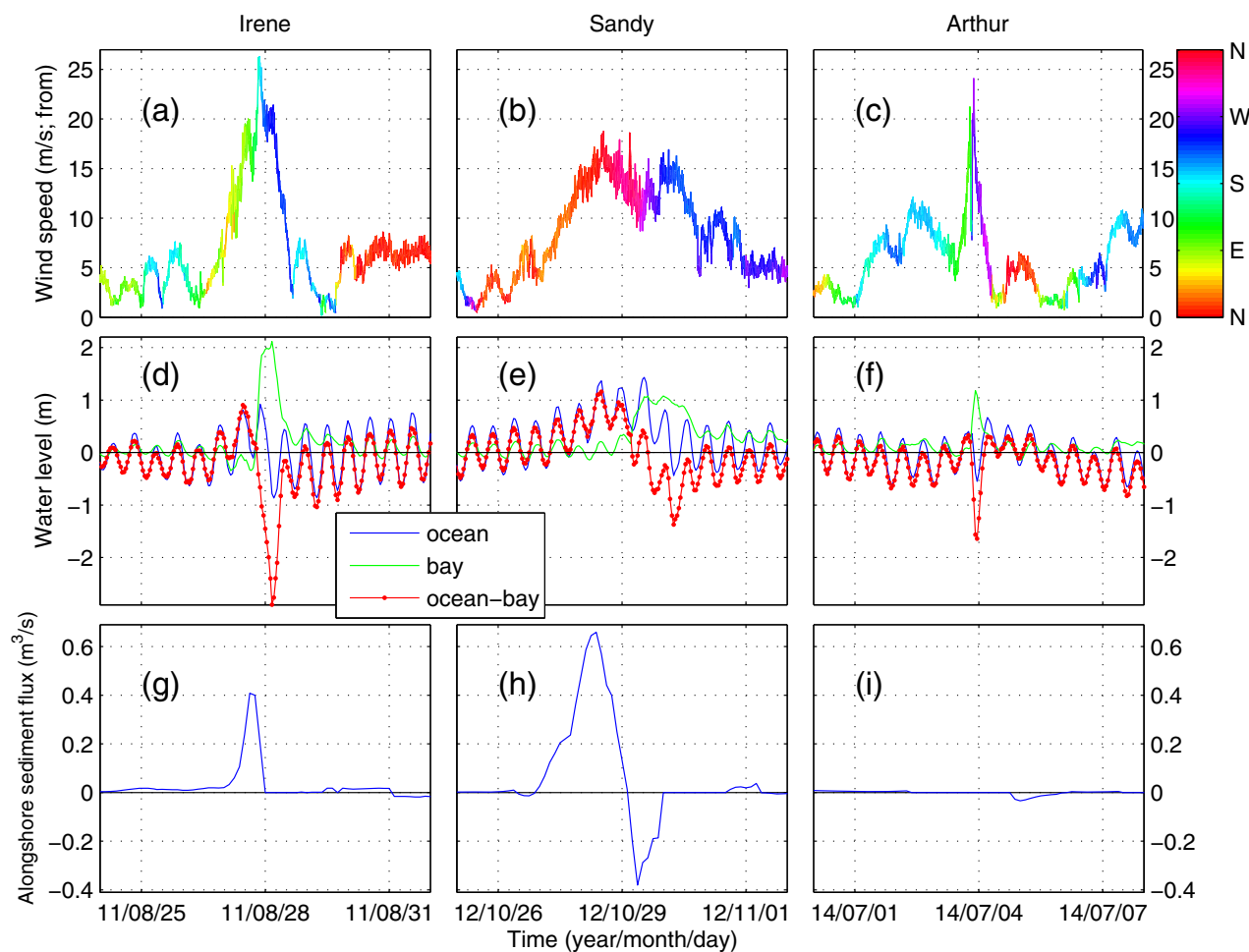
**Figure 9.** General conditions during the three hurricanes that impacted the Pea Island breach between January 2011 and January 2016. Left, middle, and right plots correspond to Hurricanes Irene, Sandy and Arthur, respectively. (a–c) Wind speed and direction (colors indicate the direction winds are from; e.g., red means Northerly winds); (d–f) water levels at the bay (green) and the ocean (blue), and the water level difference (dotted red; positive difference means the ocean water level is higher than the bay); and (g–i) estimates of sediment transport rate along the Pea Island breach (positive indicates Northward, negative indicates Southward transport).

25 ms$^{-1}$ and were from South, Southwest, and West during the peak (Figure 9a). The wind pushed the water toward the North in Pamlico Sound and caused the bay side water level to be 2.1 m with respect to NAVD 88 and the ocean side was about −0.9 m with respect to NAVD 88 (Figure 9d). Wave setup at the ocean side [*Stockdon et al.*, 2006] was estimated to be 0.8 m which would bring the water level at the ocean side to −0.1 m with respect to NAVD 88 at the peak of the Hurricane. These created a 2.2 m difference in sea level elevation between the bay and the ocean (Figure 9d). The dune height near Pea Island before Hurricane Irene was 1.9 m with respect to NAVD 88 (Figure 3), which was a local minimum within the 10 km neighborhood of the Island [*Hardin et al.*, 2012]. It is possible that wave setup inreased the vulnerability of the dunes, however, a large-scale assessment of coastal change due to Irene (http://coastal.er.usgs.gov/hurricanes/irene/coastal-change/updated-assessment.php) shows that only 15% of the coast near Pea Island had the probability of overwash. These suggest that the Pea Island breach most likely opened from the bay side during Hurricane Irene in August 2011 (Figures 2a and 3). Offshore waves from SSE-SE (7.5 m height and 13 s period; Figure 5) made the alongshore sediment flux along the Pea Island be dominantly northward (Figure 9g) during Hurricane Irene.

The observations during Hurricane Sandy show a different pattern. Winds were weaker (<20 ms$^{-1}$) and they were first from the north and then switched to be from the west during the second peak (Figure 9b). This shift first caused the ocean side to be about 1.1 m higher and then the bay side to be about 1.5 m higher (Figure 9e). Therefore, it is possible that the flow during both of these periods contributed to the widening of the channel due to Hurricane Sandy in October 2012 (Figures 2c and 2d). Another effect of

Hurricane Sandy, different from Irene, in the area is the overwash into the bay side, evident from the aerial photographs (Figures 2c and 2d). The sediment transport along Pea Island was also greater than those estimated for Irene, due to more-energetic and longer-period waves offshore (8 m height and 14 s period; Figure 5), first northward and switched direction to southward (Figure 9h) due to gradually changing wave direction.

Hurricane Arthur had wind direction patterns somewhat similar to those observed during Hurricane Irene but the event was weaker and of shorter duration (Figure 9c). The water level variations were also similar to Irene (but of smaller magnitudes) which suggest that Arthur opened the breach from the bay side as well (Figure 9f). Compared to Irene and Sandy, the alongshore sediment transport estimates were negligible, due to relatively small wave energy reaching the coast (offshore waves at the peak propagating to NNE), except a relatively small southward component in the wake of the Hurricane (Figure 9i).

Along-channel sediment fluxes are estimated for the periods when the breach was open (Figure 4c). Along-channel sediment fluxes follow the ocean-bay water level differences they are based on (Figure 4b; equations (5) and (6)) but their peaks are more prominent due to the combined effects of increasing channel depth and channel width during strong events. Alongshore sediment fluxes range from $-0.48$ to $0.66$ m$^3$s$^{-1}$ (i.e., toward both the south and the north along the coast) with peaks aligning with major storm events (Figure 4d). The alongshore sediment fluxes demonstrate an inter-seasonal variability with lower magnitudes during spring and summer and larger during fall and winter, however, extreme events occurred at various times year-round.

## 5. Discussion and Summary

For the process that tends to close the breach, Figure 10a shows the cumulative gross sediment volume transported alongshore. The gross alongshore sediment transport is a measure of how much sediment is deposited in the breach. The closure potential of the breach is considered the same no matter if the alongshore sediment transport is toward the North or the South. The cumulative gross alongshore sediment transport shows several rate changes and event scale increases. Between the opening from Hurricane Irene to the widening from Hurricane Sandy the cumulative gross alongshore transport rate was about 400 K m$^3$yr$^{-1}$. During the time from post-Sandy to closure of the breach (which occurred between 7 March and 13 April 2013; Figures 2e and 2f) the rate was approximately 600 K m$^3$yr$^{-1}$, or 50% greater than the earlier time period (Figure 10a). This is a likely reason for the inlet closure in the end of this period, rather than between Irene and Sandy. The higher rate of cumulative gross alongshore sediment transport between post-Sandy and the breach closure can be partly attributed to the event between 7 and 12 March 2013 that transported 70 K m$^3$ of sediment along the coast (Figure 10a). For along-channel transport, the gross sediment transport is a measure of the scour in the breach. Both landward and seaward sediment transports have the potential to scour out the breach channel. The cumulative gross along-channel sediment transport (Figure 10b) changes only during periods when the breach was open, starting with Hurricane Irene when it first opened. No transport is estimated for the periods when the breach was closed (horizontal parts of the curve in Figure 10b). In spite of less information available for post-Arthur conditions, the facts that cumulative gross along-channel transport has very similar rates of change (about 260 K m$^3$yr$^{-1}$) during the two open periods between 2011 and 2016 (Figure 10b) and that the breach was likely to be narrower due to weaker forcing during Arthur make it unsurprising that the breach took a much shorter duration and much smaller cumulative gross alongshore sediment transport to close. In low-wave-energy and weak alongshore transport environments such as embayed beaches, previous studies [*Ranasinghe et al.*, 1999; *Ranasinghe and Pattiaratchi*, 2003] highlighted possible importance of cross-shore flows in inlet closure. In our study site which is a wave-energetic, open, straight coast inlet through a barrier island, on the other hand, the most likely source of sediment to inlet for closure is alongshore transport, as also noted by *Smith and Zarillo* [1988], *De Swart and Zimmerman* [2009], and *Behrens et al.* [2013].

Aerial photographs are used for interpreting both the impacts of the three hurricanes on the Pea Island and also the overall competition between breach opening and closure processes between 2011 and 2016. Figure 2a shows that initially there were two openings created during Hurricane Irene on 28 August 2011, the smaller of which closed in about one week. The next photograph from the beginning of November 2011 (Figure 2b), taken at the end of a one-week-long period with strong northerly winds (reaching 17 ms$^{-1}$ with
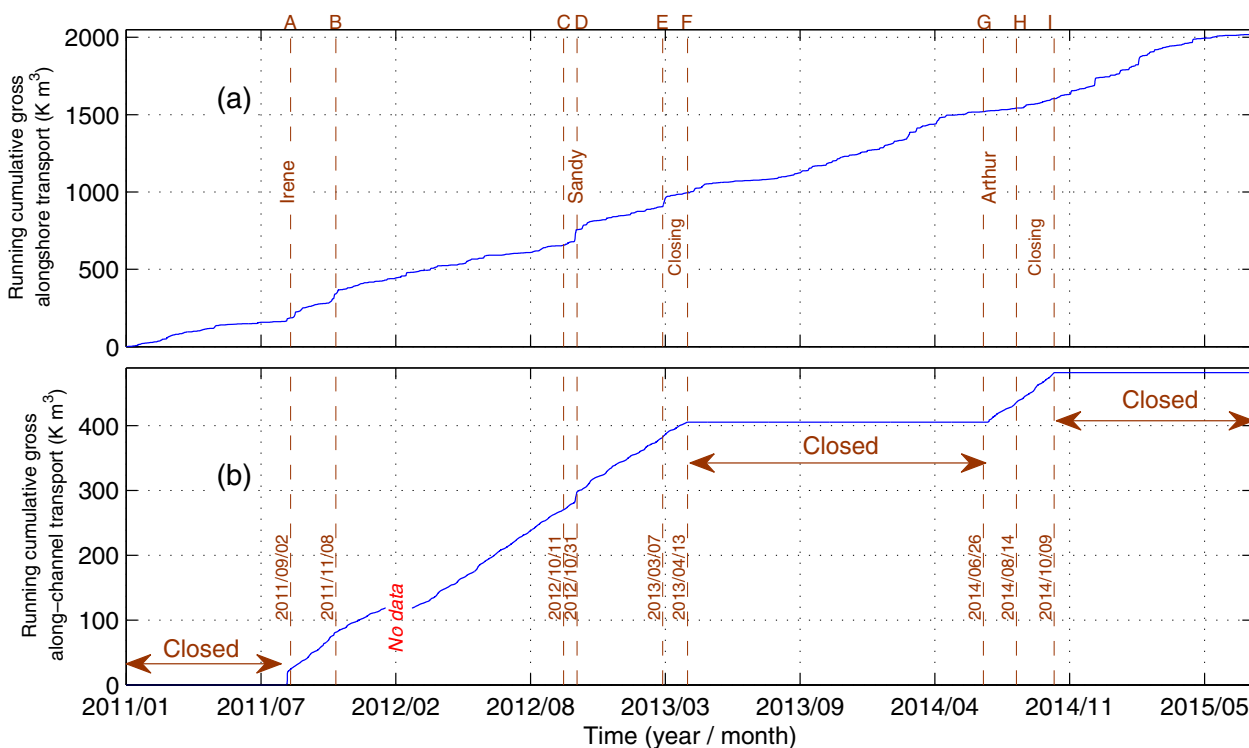
**Figure 10.** (a) Running cumulative of the gross alongshore sediment transport magnitude; (b) running cumulative of the gross along-channel sediment transport magnitude. Along-channel sediment transport on Figure 10b changes only during the periods when the breach was open; the parts of the curve that are horizontal indicate closed periods with no along-channel transport. The gap in the curve on Figure 10b is because of the absence of water level observations between January and February 2012. Capital letters at the top of the figure and the brown dashed lines correlate the dates of the photographs shown in Figure 2.

a one-week-average of 7.2 ms$^{-1}$; Figure 4a) and resulting Southward transport (Figure 4d), shows accretion at the North side of the breach and some erosion at the South side.

The next photograph (Figure 2c) was taken three weeks before Hurricane Sandy (11 October 2012), following a winter of net southward transport and a relatively calm summer and early fall in 2012 except a couple peaks of southward transport (Figure 4d). This photograph shows the channel became narrower through accretion on the north side of the breach, suggesting southward transport and also that the breach had a closure tendency. Hurricane Sandy on 29 October 2012 quadrupled the width of the narrowest part of the channel mouth (even wider than post-Irene shown in Figure 2a), and also caused significant overwash into the bay side (31 October 2012; Figure 2d). Four months after this, the channel became narrower (7 March 2013; Figure 2e) and the breach closed sometime between 7 March and 13 April 2013 (Figure 2f). Interestingly, the last photograph before the closure was taken on 7 March 2013, right before a relatively strong event between 7 and 12 March 2013. The southward transport estimated for this event is one of the largest for the studied period, after those for Irene and Sandy (Figure 4d). Therefore, it is possible that this event had a concluding impact on the closure of the breach. The breach stayed closed for 14 months, until the end of June 2014 (Figure 2g). Hurricane Arthur on 4 July 2014 briefly opened it again (Figure 2h). The post-Arthur photograph shown here was taken five weeks after the Hurricane (14 August 2014; Figure 2h). Although this photograph does not show a fully open breach, a commercially available but not open source photograph of the area taken on 5 July 2014 shows that the Pea Island breach opened due to Hurricane Arthur. The breach is closed in the photograph taken on 9 October 2014 (Figure 2i) and is still closed in the two photographs taken in June 2015 and December 2015.

In summary, under natural conditions with no human intervention, the compensating balance between along-channel pressure gradient driven flows during extreme events to keep breaches open and along-shore sediment fluxes to close breaches is identified. We demonstrated that these processes are dynamic and episodic. These findings on these processes and the changing balance between them could be applicable to many new, undredged inlets. Further insight to their dynamics and generalizing to predict the closure

of inlets elsewhere would require detailed observations. More advanced process-based modeling of the inlet morphodynamics [e.g., *Nahon et al.*, 2012] could also help to further evaluate the findings here on the breach opening and closure processes. This is not in the scope of our study due to model-related uncertainties (parametrizations, boundary conditions, etc.) and the absence of high-resolution quantitative observations of inlet geometry. Instead, the focus has been on the hydrodynamic observations near the breach together with the estimation of sediment fluxes using simplified momentum balances and analyzing these results together with the aerial photographs of the breach.

## References

Ashton, A. D., and A. B. Murray (2006), High-angle wave instability and emergent shoreline shapes: 1. Modeling of sand waves, flying spits, and capes, *J. Geophys. Res.*, *111*, F04011, doi:10.1029/2005JF000422.

Behrens, D. K., F. A. Bombardelli, J. L. Largier, and E. Twohy (2013), Episodic closure of the tidal inlet at the mouth of the Russian River––A small bar-built estuary in California, *Geomorphology*, *189*, 66–80.

Bruun, P., and F. Gerritsen (1960), *Stability of Coastal Inlets*, North-Holland, Amsterdam.

Castelle, B., J. Bourget, N. Molnar, D. Strauss, S. Deschamps, and R. Tomlinson (2007), Dynamics of a wave-dominated tidal inlet and influence on adjacent beaches, Currumbin Creek, Gold Coast, Australia, *Coastal Eng.*, *54*, 77–90.

Clinch, A. S., E. R. Russ, R. C. Oliver, H. Mitasova, and M. F. Overton (2012), Hurricane Irene and the Pea Island Breach: Pre-storm characterization and storm surge estimation using geospatial technologies, *Shore Beach*, *80*, 1–10.

De Swart, H. E., and J. T. F. Zimmerman (2009), Morphodynamics of tidal inlet systems, *Annu. Rev. Fluid Mech.*, *41*, 223–229.

Hardin, E., H. Mitasova, and M. Overton (2012), GIS-based analysis of storm vulnerability change at Pea Island, NC, paper presented at 33rd International Conference on Coastal Engineering, Santander, Spain.

Hill, A. E. (1994), Fortnightly tides in a lagoon with variable choking, *Estuarine Coastal Shelf Sci.*, *38*, 423–434.

Kraus, N. C., K. Patsch, and S. Munger (2008), Barrier beach breaching from the lagoon side, with reference to Northern California, *Shore Beach*, *76*, 33–43.

Kurum, M. O., M. Overton, and H. Mitasova (2012), Land cover and sediment layers as controls of inlet breaching, paper presented at 33rd International Conference on Coastal Engineering, Santander, Spain.

Madsen, O. S., and W. D. Grant (1976), Quantitative description of sediment transport by waves, in *Proceedings of 15th International Conference on Coastal Engineering*, pp. 1093–1112, Honolulu, American Society of Civil Engineers, New York, N. Y.

Meyer-Peter, E., and R. Mueller (1948), Formulas for bedload transport, in *Report on the 2nd Meeting International Association Hydraulic Structure Research*, pp. 39–64, Stockholm.

Nahon, A., X. Bertin, A. B. Fortunato, and A. Oliveira (2012), Process-based 2DH morphodynamic modeling of tidal inlets: A comparison with empirical classifications and theories, *Mar. Geol.*, *291-294*, 1–11.

Nichols, C. R., and L. J. Pietrafesa (1997), Oregon Inlet: Hydrodynamics, volumetric flux and implications for larval fish transport, *Rep. DOE/ ER/61425–T3*, USDOE Off. of Energy Res., Washington, D. C., doi:10.2172/479074

Overton, M. F., and E. A. Smyre (2013), Evolution of the Pea Island Breach, Outer Banks, North Carolina, *Shore Beach*, *81*, 23–27.

Poppe, L. J., K. Y. McMullen, S. J. Williams, and V. F. Paskevich (2014), USGS east-coast sediment analysis: Procedures, database, and GIS data, *U.S. Geol. Surv. Open File Rep., 2005-1001*. [Available at http://pubs.usgs.gov/of/2005/1001; http://coastalmap.marine.usgs.gov/ FlexWeb/national/usseabed/.]

Ranasinghe, R., and C. Pattiaratchi (2003), The seasonal closure of tidal inlets: Causes and effects, *Coastal Eng. J.*, *45(4)*, 601–627.

Ranasinghe, R., C. Pattiaratchi, and G. Masselink (1999), A morphodynamic model to simulate the seasonal closure of tidal inlets, *Coastal Eng.*, *37*, 1–36.

Smith, G. L., and G. A. Zarillo (1988), Short-term interactions between hydraulics and morphodynamics of a small tidal inlet, Long Island, New York, *J. Coastal Res.*, *4*, 301–314.

Stigebrandt, A. (1980), Some aspects of tidal interaction with fjord constrictions, *Estuarine Coastal Mar. Sci.*, *11*, 151–166.

Stockdon, H. F., R. A. Holman, P. A. Howd, and A. H. Sallenger Jr. (2006), Empirical parameterization of setup, swash, and runup, *Coastal Eng.*, *53*, 573–588.

Tolman, H. L. (2009), User manual and system documentation of WAVEWATCH III version 3.14, *Tech. Note 276*, 220 pp., Natl. Oceanic and Atmos. Admin., Natl. Weather Serv., Natl. Cent. for Environ. Predict., Camp Springs, Md.

Tung, T. T., D.-J. R. Walstra, J. V. D. Graaff, and M. J. F. Stive (2009), Morphological modeling of tidal inlet migration and closure, Proceedings of the 10th International Coastal Symposium, *J. Coastal Res.*, SI 56, 1080–1084.

Velasquez, L., E. Sciaudone, H. Mitasova, and M. Overton (2015), Multi-temporal geospatial analysis of the evolution and closing of Pea Island Breach, NC, in *Proceedings of Coastal Sediments'15*, pp. 1–11, World Sci., Singapore.

Walton, T. L., and W. D. Adams (1976), Capacity of inlet outer bars to store sand, in *Proceedings of 15th International Conference on Coastal Engineering*, pp. 1919–1937, American Society of Civil Engineers, New York, N. Y.

Willmott, C. J., S. G. Ackleson, R. E. Davis, J. J. Feddema, K. M. Klink, D. R. Legates, J. O'Donnell, and C. M. Rowe (1985), Statistics for the evaluation and comparison of models, *J. Geophys. Res.*, *90*(C5), 8995–9005.